# Reconstructing the Early Permian tropical climates from chemical weathering indices

Jianghai Yang[1], Peter A. Cawood[2,3], Yuansheng Du[1], Wenqian Li[4], Jiaxin Yan[1]

[1] State Key Laboratory of Biogeology and Environmental Geology & School of Earth Sciences, China University of Geosciences, Wuhan, 430074, China

[2] Department of Earth Sciences, University of St. Andrews, North Street, St. Andrews KY16 9AL, Scotland UK

[3] Centre for Exploration Targeting, School of Earth and Environment, University of Western Australia, Crawley, WA 6009, Australia

[4] No.4 Institute of Geological & Mineral Resources Survey of Henan, Zhengzhou, 450016, China

**Abstract**

Paleoflora studies suggest continental drying associated with the Early Permian deglaciation in southern North America, but not in North China. Both regions occupied tropical latitudes during the Early Permian, but were separated by the Tethys Ocean. To further constrain the tropical paleoclimate conditions during the Early Permian glacial to deglacial transition, we undertook a weathering geochemistry study on Early Permian mudstone and siltstone samples from southeastern North China and evaluated the climate impact on regional weathering patterns. Whole-rock major and trace element geochemistry, and XRD mineralogy data, suggest that sample compositions, and resultant calculated values of most weathering indices, are dominated by chemical weathering from a source akin to the average upper crust of the adjoining southern North China craton. Values of the chemical index of alteration (CIA) and other well-correlated weathering indices, including the index of sodium depletion fraction ($\tau_{Na}$), indicate high chemical weathering intensity (e.g., CIA > 80 and $\tau_{Na}$ < -0.80) in the southern North China craton source region related to intense climate forcing. Based on modern surface weathering data from granitic landscapes, we propose that the dependence of land surface soil chemical weathering intensity on the air temperature can be described by a $\tau_{Na}$-MAT (mean annual temperature) transfer function, where humidity control is demonstrated by the consistently high $\tau_{Na}$ values of surface soils on sites with small annual

precipitation rates (<400 mm/a) despite temperature variation. By applying this modern weathering-climate relationship, we compare the Early Permian (Asselian-Sakmarian) terrestrial climate between North China and west tropical Pangea. Using the southern North China craton as an average source composition, the average $\tau_{Na}$ value ~-0.90 for the Asselian-Sakmarian sediments of North China transforms to a MAT of ~20 ± 2.7 °C and suggests a warm-humid climate. Using average upper continental crust (UCC) as an average source composition, the Asselian-Sakmarian loessites in west Colorado have an average $\tau_{Na}$ value ~-0.20, which either denotes an arid climate or corresponds to a cold (or cold-dry) climate with MAT of ~4 ± 2.7 °C. If valid, this estimated MAT is consistent with inferred upland glaciation within ancestral Rocky Mountains of west tropical Pangea. The $\tau_{Na}$-MAT transfer function provides a quantitative method for deep-time paleoclimate study and enhances our understanding of the dependence of continental chemical weathering on climate conditions.

## INTRODUCTION

The demise of the late Paleozoic ice age marks the gradual collapse of high-latitude Gondwana ice sheets (Fielding et al., 2008; Isbell et al., 2012) and represents the only vegetated icehouse-to-greenhouse transition on Earth (Montañez and Poulsen, 2013). The transition was associated with significant environmental, biological and climatic changes including atmospheric $pCO_2$ increase, flora replacement, global warming, and continental aridification (Hilton and Cleal, 2007; Montañez et al., 2007; Tabor et al., 2008). Studies of paleosols, eolianites, evaporates, flora, and sedimentology from equatorial west Pangea, corresponding to present-day southern North America, have demonstrated a semiarid-arid climate during the Early Permian deglaciation (DiMichele et al., 2009; Hilton and Cleal, 2007; Soreghan et al., 2014b; Tabor et al., 2008). Both high soil temperatures in north-central Texas (Tabor, 2007) and inferred tropical upland glaciation in ancestral Rocky Mountains (Soreghan et al., 2008, 2014a) have been argued for this interval. Loessite-paleosol accumulations in western United States indicate weak continental chemical weathering (Soreghan et al., 2007, 2014b). In contrast, widespread deposition of Early Permian coal-bearing strata, as well as

the distribution of wetland plants, implies a warm, wet (tropical) environment in the eastern area of the Paleo-Tethys region, such as in North China (Hilton and Cleal, 2007; Tabor and Poulsen, 2008; Wang, 2010; Wang and Pfefferkorn, 2013; Zhang et al., 1999). To further constrain the climate conditions, a direct climate comparison study based on weathering proxy data between west Pangea and North China tropical environments is undertaken herein.

Sediment generation is controlled largely by continental weathering (e.g., McLennan, 1993), a process involving primary mineral decomposition and mobile element release (Nesbitt et al., 1980; Wilson, 2004), and is sensitive to climate and tectonic processes (Jacobson et al., 2003; Nesbitt et al., 1997; Nesbitt and Young, 1982; Rasmussen et al., 2011; Riebe et al., 2001, 2004; White et al., 1995). Numerous studies have attempted to quantify the intensity of rock chemical weathering based on geochemical compositions of resultant soils and derived sediments/sedimentary rocks and have resulted in the development of various chemical weathering indices (Fedo et al., 1995; Gaillardet et al., 1999; Harnois, 1988; Meunier et al., 2013; Nesbitt and Young, 1982; Parker, 1970; Riebe et al., 2004; Ruxton, 1968). In general, intense chemical weathering corresponds with a warm and humid climate. This relationship between weathering and climate is, however, influenced by tectonic controls on the processes of source chemical weathering through physical erosion and thus the soil residence time (Gaillardet et al., 1999; Johnsson, 1993; Nesbitt and Markovics, 1997; Nesbitt and Young, 1996; White and Blum, 1995), which in turn may be reflected in the sedimentary tectonic settings (Cawood et al., 2012). Compositions of sedimentary rocks for calculating chemical weathering index values are directly related to the source rock composition, sedimentary sorting and recycling, and post-depositional diagenesis (Cox et al., 1995; Fedo et al., 1995; Garzanti et al., 2013; McLennan et al., 1993; Nesbitt et al., 1996; Nesbitt and Markovics, 1997). Despite these factors complicating their applicability (Chetelat et al., 2013; Clift et al., 2014; Garzanti et al., 2014; Xiao et al., 2010), weathering indices have been successfully used to measure source weathering intensity of fine-grained sedimentary rocks and thus constrain deep-time climatic variation (Fedo et al., 1997a; Rieu et al., 2007; Schatz et al., 2015; Scheffler et al., 2003; Yan et al., 2010; Young et al., 2004; Young and Nesbitt, 1999). This study compiles multiple weathering indices to estimate the source chemical weathering intensity of the Early Permian strata in North China. Mineralogical and

geochemical analyses were combined to evaluate the potential influences (provenance, sedimentary recycling and sorting, post-depositional diagenesis, and physical erosion) and determine the impact of climatic variables (precipitation and temperature) on weathering intensity. These data are then used to develop a proxy for climatic conditions, which we then use to make a direct comparison between the time equivalent records from the ancestral Rocky Mountain region of western tropical Pangea and southern North China (Fig. 1). This proxy could be used as a quantitative estimate of deep-time continental surface temperature.

## SAMPLING FROM NORTH CHINA AND ANALYTICAL METHODS

North China occupied a near equatorial latitude during the Pennsylvanian-Early Permian (5-15°N; Embelton et al., 1996; Huang et al., 2001; Zhu et al., 1996) and was surrounded by the warm waters of the Tethys Ocean to the west and the Panthalassic Ocean to the east (Fig. 1; Torsvik and Cocks, 2004). In North China, the Pennsylvanian-Early Permian strata accumulated in a stable, cratonic basin and disconformably overly Cambrian-Ordovician carbonate rocks (Wang, 1985; Wang and Mo, 1995). From oldest to youngest, this succession includes the Benxi, Taiyuan, Shanxi, and Xiashihezi formations. Two drill core sections (Zk1401 and Zk0901) were analyzed from the Yongcheng Coalfield of eastern Henan Province in southeastern North China (Fig. 2A, B). The studied cored intervals consist of the upper Shanxi Formation and the conformably overlying Xiashihezi Formation. The cored sedimentary rocks consist of black-gray mudstones, siltstones and fine sandstones along with several coal seams (Fig. 2C, D). The sediments accumulated in a deltaic environment (Feng, 2012). Zircon U-Pb dating of a tuff from near the top of the Shanxi Formation gave an age of 293 ± 2.5 Ma (Yang et al., 2014). In combination with regional biostratigraphic data (Wang, 1982; Wang and Zhang, 1985; Zhang, 1990), this age constrains the Shanxi Formation to the Asselian-Sakmarian and the Xiashihezi Formation to the Artinskian-Kungurian (Gradstein et al., 2012). This succession covers the Early Permian glacial-postglacial transition and correlates with contemporaneous high-latitude Gondwana sequences, and is an interval that corresponds with the global late Sakmarian-early Artinskian enhancement in continental weathering (Yang et al., 2014).

Bulk-rock geochemical and mineralogical XRD data were measured on core samples,

including 33 silt-mudstone and 2 fine sandstone samples from Core Zk1401 (Fig. 2C), and 36 silt-mudstone samples from Core Zk0901 (Fig. 2D), which is located ~40 km southwest of Zk1401 (Fig. 2B). After eliminating any surface contamination, samples were ground to less than 200 mesh. For elemental oxide concentration analysis, sample powders were mixed with dry lithium tetraborate and borate and fused to glass beads. Analyses were conducted on a PANalytical Axios X-ray florescence spectrometer at ALS Chemex (Guangzhou, China). Analytical accuracy is better than 5% and uncertainty less than 5%. Trace element abundances of Core Zk1401 samples were obtained on a Perkin Elmer Elan 9000 inductively coupled plasma-mass spectrometer (ICP-MS) at ALS Chemex (Guangzhou, China). Accuracy is better than 10% and uncertainty less than 10% for the majority of analyzed elements. For Core Zk0901 samples, trace element abundances were measured on an Agilent 7500a ICP-MS at the State Key Laboratory of Geological Process and Mineral Resources (GPMR), China University of Geosciences (Wuhan). About 50 mg of each sample powder was weighed into a Teflon bomb and then digested by HF + $HNO_3$. Analytical precision and accuracy are generally better than 5% for most trace elements. Mineralogical XRD studies for all samples were performed with a PANalytical X'Pert Pro model instrument using a Cu-Ni tube at 40 kV and 40 mA at GPMR, China University of Geosciences (Wuhan). Samples were continuously scanned from 3 to 65° (2θ) with a speed of 25°/min using CuKα radiation and a graphite monochromator. The analytical software package for the XRD analysis is X'Pert HighScore Plus. The mass percentage of the main mineral phases identified is semi-quantified with an analytical error of 5-10%.

# RESULTS

## Mineralogical and chemical compositions

XRD mineralogical and geochemical data for Core Zk1401 samples were compiled from Yang et al. (2014) and some additional trace element concentrations are given here. New whole-rock geochemical and XRD mineralogical results for Core Zk0901 samples are first reported in this study. All the mineral and chemical composition data for the samples of the

two cores are collectively listed in Tables DR1-2[1]. Quartz and clay minerals are the major detrital components with only very minor feldspar and calcite (Fig. 3). Most of the samples contain siderite, occurring as oolites, and 5 of the samples (Ps7, Ps20, Ps33, C14-156 and C14-157) have high siderite contents (15-46 %). Clay minerals include chlorite, illite and kaolinite. Kaolinite is the main clay phase (40-80 %) and is negatively correlated with both illite (0-40 %) and chlorite (5-35 % generally, but 55-65% for samples Ps36 and Ps37). Samples rich in siderite or chlorite have $Fe_2O_{3T}$ contents of 12.4-37.5 % with all other samples having values of < 6 % except Sample Ps8 (8.7 %). Normalized to the average upper crust composition of southern North China (SNC, Gao et al., 1998), the Eu/Eu*, Ce/Ce* and $(La/Yb)_N$ ratios of the analyzed samples have average values of 0.95, 1.05 and 1.02, respectively, but each has a relatively wide range of values.

**Weathering index values**

Weathering indices can be used to quantitatively trace weathering history based on the chemical composition of weathered materials (Reiche, 1943; Ruxton, 1968; Price and Velbel, 2003). A variety of chemical weathering indices were compiled in this study (supplementary data file) and detailed formulations for index calculations are listed in Table 1. These indices involve different elements and thus can be combined to discuss the potential influences on sediment compositions. For example, CIA (chemical index of alteration, Nesbitt and Young, 1982) and elemental weathering indices $\alpha_K$ and $\alpha^{Al}_K$ (Gaillardet et al., 1999; Garzanti et al., 2013) are sensitive to potassium metasomatism, which has no effect on other indices like CIW (chemical index of weathering, Harnois, 1988). WIP (weathering index, Parker, 1970) and $\tau_{Na}$ (sodium depletion fraction, Rasmussen et al., 2011) are sensitive to sedimentary recycling and sorting induced accumulation of quartz and zircon, which generally does not affect CIA value (Garzanti et al., 2013). The upper crust of southern North China craton (SNC, Gao et al., 1998) is considered the dominant source for the analyzed Early Permian sediments (Yang et al., 2014) and its average composition is used for the calculation of weathering indices requiring source rock composition. The calculated values of compiled weathering indices for the analyzed silt-mudstone samples are listed in Table DR3. The

[1] Supplementary information (outline of compiled weathering indices and Tables DR1-4) is available online at http://www.geosociety.org/pubs/ft21xx.htm

majority of weathering indices, like WIP, CIW, $R^{3+}/(R^{3+}+R^{2+}+M^{+})$ (trivalent-cations enrichment index, Meunier et al., 2013), LCWP (loss chemical weathering proxy, Yang et al., 2006), $\tau_{Na}$ and some elemental weathering indices (e.g., $\alpha_K$, $\alpha^{Al}_{Na}$ and $\alpha^{Al}_{K}$; Gaillardet et al., 1999; Garzanti et al., 2013), have good correlations with CIA (Table 2, Fig. 4). Stratigraphic variation trends for seven representative indices (CIA, CIW, WIP, LCWP, $\alpha_K$, $\alpha^{Al}_{K}$ and $\tau_{Na)}$ through the upper Shanxi to Xiashihezi formations are shown on Figure 3. Overall, the analyzed samples have high CIA (>80), CIW (>90) and $\alpha_K$ (>2), $\alpha^{Al}_{K}$ (>2) values, and low WIP (<30), LCWP (<4) and $\tau_{Na}$ (<-0.80) values.

Here we pay specific attention to the sodium chemical depletion index ($\tau_{Na}$). Sodium is found predominantly in plagioclase in granites and is not significantly incorporated into clays in most regolith. This index quantifies the net Na loss relative to Zr during chemical weathering and has been used to measure the intensity of modern weathering profiles (Rasmussen et al., 2011). The $\tau_{Na}$ values of land surface soils generally covary with local or regional climatic conditions: mean annual precipitation rate (MAP) and mean annual atmospheric temperature (MAT) (Rasmussen et al., 2011). The relationship between land surface soil $\tau_{Na}$ values and regional MAT will be explored further by using an extended dataset compiled in this study (Table DR4). Error propagation for $\tau_{Na}$ can be calculated based on the analytical uncertainties associated with the measurements of $Na_2O$ (<5%) and Zr (<10%). Following the simple error propagation rule (Taylor, 1997) as used by Rasmussen et al. (2011), the calculated relative standard deviation for $\tau_{Na}$ would be less than 11%. This uncertainty does not affect our final $\tau_{Na}$-based climate interpretation.

# DISCUSSION: LINKING CHEMICAL WEATHERING WITH CLIMATE

## Provenance interpretation

For in situ weathered profiles on metamorphic (Price and Velbel, 2003) and magmatic rocks (Kamei et al., 2012), protolith heterogeneity influences the reliability of weathering indices. For sediments, their compositions are directly related to the provenance from which they were derived (Johnsson, 1993; McLennan et al., 1993). A graphic provenance interpretation based on an A-CN-K ($Al_2O_3$-$Na_2O$+CaO*-$K_2O$) diagram was proposed by Fedo et al. (1995) and has been widely applied (e.g., Clift et al., 2014; Rieu et al., 2007; Yang

et al., 2012a; Young and Nesbitt, 1999). On this triangular diagram, those samples that have undergone a moderate degree of weathering (CIA <~86) generally display a trend (sub)parallel to the A-CN boundary, and after approaching the A-K boundary those samples having undergone an advanced degree of weathering (CIA>~86) move toward the A apex (Fig. 5A). This trend mimics the natural weathering trend for modern moderate-advanced weathered profiles on igneous rocks and the predicted weathering trend based on thermodynamic calculations (Nesbitt and Young, 1984). This linear trend for the intermediately weathered samples can be extended very close to the point representing the average upper crust composition of the southern North China craton (SNC, Gao et al., 1998). Such a pattern combined with the paleogeographic analysis (Wang, 1985) is consistent with a SNC-dominated provenance for this sedimentary sequence (cf. Yang et al., 2014). Contribution from the upper crust of the interior North China carton (INC, Gao et al., 1998) is also highly possible, but seems limited in the paleogeographic reconstruction (Wang, 1985). This conclusion is also supported by the plots of the analyzed samples on the SNC-4Si line in the $M^{+}$-4Si-$R^{2+}$ triangle (Meunier et al., 2013; Fig. 5B), on the SNC-AF line in the AF-CNK-M ($Al_2O_3$+$Fe_2O_{3T}$-CaO*+$Na_2O$+$K_2O$-MgO) ternary diagram proposed by Babechuk et al. (2014; Fig. 5C), and along the chemical weathering trend of SNC on the $R^{3+}/(R^{3+}+R^{2+}+M^{+})$-$\Delta$4Si% diagram (Meunier et al., 2013; Fig. 5D). These plots indicate a general weathering trend for a source region with average upper crust composition of southern North China craton. Though the Zr/Ti and $Al_2O_3/TiO_2$ ratios often used as provenance indicators are different from sample to sample, and are comparable or higher in samples than in SNC, the samples have average SNC normalized Eu/Eu*, Ce/Ce* and $(La/Yb)_N$ ratios close to 1. Consistent with this provenance interpretation, the calculated SNC source rock-based weathering indices like $\Delta$4Si%, $\alpha^{Al}_{E}$ and $\tau_{Na}$ have strong correlations with CIA, whose values are not based on source composition (Table 2 and Fig. 4).

**Evaluating sedimentary recycling and sorting**

As a result of sedimentary recycling, the mineralogical and chemical compositions of deposits may reflect the combined effects of syn-depositional weathering regimes as well as the effects of previous weathering and diagenetic histories (Cox et al., 1995; Gaillardet et al., 1999; Garzanti et al., 2013). In North China, late Paleozoic coal-bearing sequences

232 disconformably overly Cambrian-Ordovician marine carbonates (Wang, 1985), and thus it is
233 unlikely that the underlying strata provide a significant source of recycled siliciclastic
234 materials for the late Paleozoic basin. Furthermore, the studied Lower Permian sedimentary
235 rocks and their dominant SNC source display a well-defined polynomial CIA-WIP
236 relationship (Fig. 4A). This is consistent with derivation of first-cycled muddy sediments
237 from metamorphic and plutonic basement rocks (Garzanti et al., 2013, 2014). Poly-cyclic
238 reworking processes tend to accumulate stable minerals like quartz and zircon (McLennan et
239 al., 1993) in the sediments, diluting other components. With increasing sedimentary recycling,
240 WIP value will decrease linearly, but CIA and other indices (e.g., $\alpha^{Al}_{E}$) are largely immune to
241 this process (Garzanti et al., 2013, 2014). Although resolving recycling becomes harder as
242 weathering intensity increases (Garzanti et al., 2013, 2014), good correlation of CIA with
243 WIP combined with the regional stratigraphic framework suggests that recycling is not
244 significant for the Early Permian sedimentary system in southern North China.

245 The Al/Si ratio, used as a proxy of grain size and indicator of hydraulic sorting
246 (Bouchez et al., 2011), varies from ~0.3 to 1.0. For the analyzed Core Zk1401 samples, Al/Si
247 and quartz/clay ratios have a negative correlation ($r^2$ = 0.78, Fig. 6A). This correlation
248 suggests the ratio provides insight into the impact of sedimentary sorting processes on
249 chemical and mineral compositions of the samples, with enrichment of minerals like quartz
250 and zircon in coarse sediments and of clays in finer sediments (Cullers et al., 1988; Garzanti
251 et al., 2013; McLennan et al., 1993; Morey and Setterholm, 1997; Nesbitt et al., 1996; Singh
252 and Rajamani, 2001; Yang et al., 2012a). However, rather than an expected
253 sorting-responsible positive correlation between Al/Si and K/Si ratios (Lupker et al., 2013),
254 the two ratios have a negative correlation for Core Zk1401 samples ($r^2$ = 0.59) and show no
255 correlation for Core Zk0901 samples (data for Al/Si vs. K/Si plots not shown here).
256 Meanwhile, WIP and quartz/clay mineral ratio show a positive correlation for Core Zk1401
257 samples ($r^2$ = 0.54) or have no co-varying relationship for Core Zk0901 samples (Fig. 6B).
258 This result is strongly at odds with the sorting effect that quartz enrichment tends to dilute the
259 alkali-alkaline earth element contents and thus decrease the WIP value (e.g., Garzanti et al.,
260 2013). Even the weathering indices based on sorting-sensitive elements Zr and Ti, such as
261 LCWP, and $\tau_{Na}$, the correlation with Al/Si and quartz/clay mineral ratios are not obvious for

the studied samples (Fig. 6C-D). It is thus unlikely that sedimentary sorting process dominates during the formation of these Early Permian sediments.

**Post-depositional diagenetic alteration**

Diagenesis forms authigenic illite, chlorite and carbonate minerals during the conversion of mud sediments into mudstone (Fedo et al., 1997b; Awwiller et al., 1993; Land et al., 1997; Bloch et al., 1998), and changes the chemical composition of sedimentary products and resultant calculated weathering index values. XRD detected all three of these authigenic minerals in the Early Permian samples. Illitization, through the addition of K into mudstones (Awwiller et al., 1993; Bloch et al., 1998), decreases apparent CIA values (Fedo et al., 1995). On the A-CN-K diagram, some of our samples plot on a line parallel to the A-CN boundary mimicking the predicted weathering trend of the SNC source (Fig. 5A). This plot indicates little to no K-metasomatism, which would lead to muddy samples plotting off this trend and toward the K apex (Fedo et al., 1995; see Fig. 5A). Though CIA values of our samples are generally high and the samples falling on such a line are few, the strong correlation of CIA with CIW, CPA, LCWP and $\tau_{Na}$, which are indices that are insensitive to K-metasomatism (Tables 1 and 2, Figs. 4B, D), do not support significant influences of illitization. Chlorite accounts for 5-35% of the clay minerals for all samples except samples Ps36 and Ps37, where more than half of the clays are chlorite, and the kaolinite contents are much lower than in other analyzed mudstones. Of carbonate minerals, calcite content is always low and siderite content can be relatively high in some samples (Ps7, Ps20, Ps33, C14-156 and C14-157). Samples with relatively high siderite or chlorite contents slightly deviate from the predicted weathering trend for the source SNC (Fig. 5). Such plots suggest evident diagenetic superimposition on the source chemical weathering signals. Enrichment of these samples in Fe results from the mobilization and subsequent fixation of divalent iron in a reduced post-depositional environment. Siderite likely formed during early stages of diagenesis with $CO^{2-}$- and $Fe^{2+}$-enriched pore waters (Bojanowski and Clarkson, 2012) and chlorite formed during later deep burial diagenesis (Boles and Franks, 1979; Land et al., 1997). Thus, diagenesis increases the values of MIA-O and $R^{3+}/(R^{3+}+R^{2+}+M^{+})$, which measure the relative enrichment of Fe and Al in weathered materials, but decrease the WIP value for the authigenic Fe-minerals` dilution.

## Climatic control on source chemical weathering intensity

By excluding possible influences from provenance, sedimentary recycling and sorting, and post-depositional diagenesis, the observed elemental and mineralogical compositions can be used to monitor the chemical weathering intensity in the source region. The simplest interpretation of the strong correlations between the weathering indices, following Schatz et al. (2015), is that these indices are equally well-suited to tracing the source chemical weathering intensity for the studied Early Permian sedimentary rocks. Thus, a conclusion that can be drawn from the calculated weathering index values (e.g., CIA > 80 and $\tau_{Na}$ < -0.80) is that the chemical weathering intensity of the SNC source was relatively high. Such high source chemical weathering intensity could result from either favorable climate conditions (high temperature and humidity) or ineffective physical erosion. Physical erosion converts in-situ weathered soils to detritus, which is transported and deposited as sediments (e.g., Nesbitt et al., 1997), and in turn is related to tectonics and landscape topography (Dixon et al., 2012; Jacobson et al., 2003; Nesbitt et al., 1997; Riebe et al., 2004; West et al., 2005).

To further understand the dynamic controls of physical erosion and climatic conditions on continental surface weathering intensity, we compiled modern data from regoliths developed on granitic terrains (Burke et al., 2007, 2009; Dixon et al., 2012; Khomo, 2008; Rasmussen et al., 2011; Riebe et al., 2004; White et al., 2001;). This dataset is from 56 weathering sites distributed in low-middle latitudes (~15-42° N/S, Fig. 7A) with mean annual temperature (MAT) of -0.4 to 25 °C and mean annual precipitation (MAP) of 220-4200 mm/a. The physical erosion rates for these regolith sites have been constrained by cosmogenic radionuclides and range from <2 to 252 m/Ma, covering all the estimated global average physical erosion rates (~10-60 m/Ma) for the Phanerozoic (Wilkinson, 2005). Available Na and Zr contents of regolith soils and corresponding bedrock are compiled from literature and used to calculate the average $\tau_{Na}$ value of soils as a measure of the land surface weathering intensity (Table DR4). Based on this dataset, we observed a strong linear correlation ($r^2$ = 0.84) between average land surface soil $\tau_{Na}$ and MAT for sites with physical erosion rate < 100 m/Ma and MAP > 400 mm/a (except four sites, Fig. 7B). In comparison, seven sites with high physical erosion rate (> 100 m/Ma, Sites JT-1, JT-4 and JT-5 in Jalisco Highland and Sites RT-1 and RT-2 in Jalisco Lowland, Mexico, and Site FR-5 from Fall River and Site A4

in Fort Sage, Northern Sierra NV) and one site (Davis Run, northern Virginia, where Zr is unavailable and Ti is used for $\tau_{Na}$ calculation, White et al., 2001) with a very low physical erosion rate (< 2 m/Ma, Rasmussen et al., 2011) display relatively higher and lower land surface soil $\tau_{Na}$ values (Fig. 7B), respectively. This discrepancy demonstrates the control of physical erosion and thus tectonic activity on land surface chemical weathering intensity (Dixon et al., 2012). Similarly, relatively higher $\tau_{Na}$ values (> -0.30) are noted for land surface soils at 8 sites (Site SR-10 in Santa Rosa Mtns NV, Sites CE-3 and JC-1 in Sonara Desert, Mexico, Sites A1, A2 and A3 in Fort Sage, Northern Sierra NV, Site NP-1 in Nichols Peak, Southern Sierra NV and Site W1 in western Sierra Nevada range of California) with MAP <400 mm/a despite a large variation of MAT and lower $\tau_{Na}$ values (< -0.70) are observed for three sites with high MAP of 4000 mm/a, but not high MAT of ~8 °C (Fig. 7). These observations suggest a threshold control of water availability on chemical weathering (Rasmussen et al., 2011). There is one site with physical erosion rate >100 m/Ma apparently fitting into the linear model (Site FR-2 from Fall River and one site in Fort Sage, Northern Sierra NV). One explanation might be the overestimate of physical erosion rate or underestimate of Na/Zr ratios in the soils. Alternatively, this fit may suggest that our linear model could be applied to some sites with high physical erosion rates.

For the analyzed sedimentary rocks, the physical erosion rate is unlikely to be very low because: (1) the southern margin of North China craton experienced significant Ordovician-Silurian orogenesis and tectonic uplift (Gao et al., 1998; Wang and Mo, 1995; Yang et al., 2012b); and (2) the early Paleozoic arc-related magmatic rocks and uplifted continental crystalline basement provided a predominant sedimentary source for the Pennsylvanian-Early Permian sequences (Wang, 1985; Wang et al., 2010). We assume the average physical erosion rate in the Southern North China source region would be comparable to, or higher than, the global average value, which was estimated at ~10-30 m/Ma in the Pennsylvanian-Early Permian (Wilkinson, 2005). Accepting this inferred physical erosion rate and the indication of weathering index values (e.g., CIA and $\tau_{Na}$) for source land chemical weathering intensity, the high SNC source chemical weathering intensity appears to result from climate forcing related to high temperature and humidity.

**Application of $\tau_{Na}$–MAT transfer function to the Asselian-Sakmarian climate in**

**southern North China and southern North America**

Based on a linear model for 36 data-sites of land surface soil $\tau_{Na}$ and MAT, an empirical $\tau_{Na}$–MAT transfer function with standard error of 2.7 °C is proposed in Figure 7. The equation is expressed as: MAT = -24.2×$\tau_{Na}$–0.9 ($r^2$ = 0.84, P < 0.0001). Although this transfer function describes the dependence of land surface chemical weathering intensity on air temperature, it might be applicable to sediments derived from the surface soils in a wider scale. For example, fine-grained sediments from the river mouth with regional or continental scale drainage and loess deposits with an extensive derivation provide a first-order representation of surface weathered materials of the upper crust (e.g., Taylor and McLennan, 1985). Therefore these sediments could provide clues for measuring the average chemical weathering intensity of the surface soils in the source region and thus archive an approximate regional or continental scale (depending on the source region) climate record. Using average upper crust of interior North China craton (INC, Gao et al., 1998) as an average source composition for the loess deposits of the Chinese Loess Plateau, $\tau_{Na}$ of ~-0.40 was calculated for the average composition of loess L1-5 from 6 sections based on the chemical data reported by Ding et al. (2001). Such a $\tau_{Na}$ value is consistent with their average CIA value of ~61 (Fig. 4D), suggesting the rationality of using INC as the average source composition and no significant sorting differentiation between the average Na and Zr concentrations in loess L1-5 (sedimentary sorting has limited effect on the average Na/Zr ratio). Accepting this $\tau_{Na}$ value, the corresponding MAT during loess deposition would be ~8.8 ± 2.7 °C. This MAT estimate is similar to ~8.6 °C based on magnetic susceptibility-MAT transfer function (Han et al., 1996) using average magnetic susceptibility of ~$70\times10^{-8}$ SI (Ding et al., 1999). On this basis we apply the $\tau_{Na}$-MAT transfer function to the sedimentary rocks of the Shanxi Formation in North China and to the Maroon Formation in western Colorado of southern North America, which was deposited in western Pangea (Fig. 1), and undertake a climate comparison between these two regions. The latter is characterized by loessite-paleosol sequences and contains acicular zircons dated at 293.1 ± 3.2 Ma, which was interpreted as indicating the stratigraphic age of the unit (Soreghan et al., 2014b). Thus, both Shanxi and Maroon formations are of Asselian-Sakmarian age, when the atmospheric $CO_2$ concentration was estimated to be similar to present-day levels (Montañez et al., 2007).

382 The Shanxi muddy sediments from North China have low $\tau_{Na}$ values with averages of
383 -0.88 and -0.89 for cores Zk1401 and Zk0901, respectively, correlating well with high CIA
384 values (Fig. 4D). The presence of multiple thick coal beds and wetland paleoflora (Wang,
385 2010; Zhang, 1999) suggest a humid climate, consistent with modeled mean annual
386 precipitation around 1000-2500 mm/a for this tropical region at $CO_2$ levels comparable to
387 present day values (355 ppmv, Poulsen et al., 2007). Therefore water availability was not
388 limiting the land surface chemical weathering in North China during this period. According to
389 the $\tau_{Na}$–MAT transfer function, the MAT is estimated at ~20 ± 2.7 °C (Fig. 7). This land MAT
390 estimate is comparable with or slightly higher than tropical annual surface temperatures
391 modeled on the basis of low $CO_2$ level with different ice sheet volumes by Poulsen et al.
392 (2007), but lower than the calculated epeiric sea surface temperatures (>24 °C assuming
393 $\delta^{18}O_{seawater}$ from 0 ‰ to +1‰) of the Tethys Ocean determined from $\delta^{18}O$ data on shell
394 materials (Chen et al., 2013; Angiolini et al., 2009). In addition, this temperature is obviously
395 lower than the estimated earliest Permian soil temperatures (~35-37 ± 3 °C), but overlaps
396 with those of the late Pennsylvanian (24 ± 3 °C) from north-central Texas of southern North
397 America (Tabor, 2007). The temperature similarity is consistent with the close affinity
398 between the Early Permian paleofloral community colonized in North China and that of the
399 late Pennsylvanian in west tropical Pangea, where the wetland floras had largely diminished
400 by the earliest Permian (Hilton and Cleal, 2007).
401 For the loessites of the Maroon Formation in west Colorado (southern North America),
402 their average geochemical composition was compiled from Soreghan et al., (2014b) and the
403 average upper continental crust (UCC) was used as the average source composition. Using
404 the three often cited UCC model compositions proposed by Taylor and McLennan (1985),
405 Condie (1993) and Rudnick and Gao (2003), the calculated average $\tau_{Na}$ value is ~-0.19,
406 ~-0.24 and ~-0.02, respectively. The third $\tau_{Na}$ value indicates very small net Na loss in the
407 loessites relative to their protolith and thus nearly no plagioclase chemical weathering. This is
408 considered unrealistic for these loessites deposited in a tropical region. The former two $\tau_{Na}$
409 values are not distinguishable considering the analytical errors and uncertainties with the
410 UCC composition models. They are consistent with low CIA value (~55, Soreghan et al.,
411 2014b; Fig. 4D), suggesting a relatively low degree of chemical weathering for the source

land surface. These $\tau_{Na}$ values are similar to that of the modern land surface soils in sites with low precipitation (Fig. 7) and thus indicate a much more arid climate as evidenced by paleosol and paleoflora studies in the tropics of western Pangea (DiMichele et al., 2009; Hilton and Cleal, 2007; Tabor et al., 2008). Alternatively, such low chemical weathering intensity might denote low air temperatures at ~ 4 ± 2.7 °C (using $\tau_{Na}$ value of -0.19, Fig. 7), suggesting a cold or cold-dry climate. Such cooler temperature would favor glacial ice accumulation on uplands of low-elevation (<1000 m) assuming an adiabatic lapse rate of ~6.5 °C/km (Soreghan et al., 2008). If our assumption is valid that the sediment compositions of the Shanxi and Maroon formations reflect the chemical weathering intensity in their source regions, the tropical climate would be warm-humid in southern North China and cold or cold-dry in southern North America.

## SUMMARY

Chemical weathering indices provide climate proxy data for the Early Permian strata (upper Shanxi and Xiashihezi formations) in southern North China Craton. Elemental concentrations and calculated weathering index values suggest that these sediments were derived from a common source with an average composition akin to the average upper crust of southern North China craton (SNC). Analyzed mudstone and siltstone samples from two drill cores lack mineral and chemical features indicative of significant influences from sedimentary recycling and sorting. Though authigenic siderite and chlorite contents are high in some samples, the effect of diagenesis is minimal as the majority of samples follow the trend of the SNC source in weathering plots. Including all the data from the two cores, as well as the potential average source composition represented by SNC, good correlations of CIA with most other weathering indices (e.g., CIW, WIP, $\Delta$4Si%, $R^{3+}/(R^{3+}+R^{2+}+M^{+})$,MIA-O, LCWP, and $\tau_{Na}$) were observed and interpreted as recording the weathering intensity in the source region. The values of these well-correlated weathering indices consistently suggest high source chemical weathering intensity. In terms of the geological evolution of the SNC source region, high chemical weathering intensity likely reflects intense climatic forcing rather than very low physical erosion rates.

Based on modern soil weathering data from worldwide granitic landscapes with

low-moderate physical erosion rate, the surface soil weathering intensity measured by the depletion of Na relative to immobile Zr (index of sodium depletion fraction, $\tau_{Na}$) is dominantly controlled by climate conditions. A linear correlation of surface soil $\tau_{Na}$ with mean annual air temperature (MAT) is demonstrated for sites where mean annual precipitation is more than 400 mm/a. According to this relationship a $\tau_{Na}$-MAT transfer function is defined and applied to the deltaic fine sediments and loess which provide a first-order representation of surface soils of a large continental region. Applying this transfer function to the Asselian-Sakmarian muddy samples in North China generates a MAT of ~20 ± 2.7 °C, which when integrated with wetland paleoflora and coal-bearing strata suggests an overall warm-humid climate in North China during this period. In contrast, the $\tau_{Na}$ values for the loessites of the Asselian-Sakmarian Maroon Formation in west tropical Pangea indicate a low chemical weathering intensity that might be attributed to limited humidity or/and a much colder climate (~ 4 ± 2.7 °C), consistent with previously inferred upland glaciation. This weathering index based climate proxy provides a method to quantitatively estimate the paleo-temperature from sedimentary records.

## ACKNOWLEDGEMENTS

This study is financially supported by the National Natural Science Foundation of China (41302083, 41572078), the National Basic Research Program of China (2011CB808800) and the Fundamental Research Funds for the Central Universities (CUGL140402), China University of Geosciences (Wuhan). We thank Shaoquan Yan (No. 4 Institute of Henan Geology) for help with sampling, Jishun Yu (GPMR, China University of Geosciences, Wuhan) for XRD mineralogical analyses, and Haihong Chen (GPMR, China University of Geosciences, Wuhan) for trace element contents analysis. Manuscript was finished during J. Yang`s visit to UK funded by China Scholarship Council (201406415003). This manuscript was significantly improved from critical reviews by the editors and two anonymous reviewers.

## References

Angiolini, L., Jadoul, F., Leng, M. J., Stephenson, M. H., Rushton, J., Chenery, S., and Crippa, G., 2009, How cold were the Early Permian glacial tropics? Testing sea-surface temperature using the oxygen isotope composition of rigorously screened brachiopod shells: Journal of the Geological Society, London, v. 166, p. 933-945.

Awwiller, D.N., 1993, Illite/smectite formation and potassium mass transfer during burial diagenesis of mudrocks: a study from the Texas Gulf Coast Paleocene-Eocene: Journal of Sedimentary Petrology, v. 63, p. 501-512.

Babechuk, M.G., Widdowson, M., and Kamber, B.S., 2014, Quantifying chemical weathering intensity and trace element release from two contrasting basalt profiles, Deccan Traps, India: Chemical Geology, v. 363, p. 56-75.

Bloch, J., Hutcheon, I.E., and de Caritat, P., 1998, Tertiary volcanic rocks and the potassium content of Gulf Coast shales—the smoking gun: Geology, v. 26, p. 527-530.

Bojanowski, M.J., and Clarkson, E.N.K., 2012, Origin of siderite concretions in microenvironments of methanogenesis developed in a sulfate reduction zone: an exception or a rule: Journal of Sedimentary Research, v. 82, p. 585-598.

Boles, J.R., and Franks, S.G., 1979, Clay diagenesis in Wilcox Sandstones of Southwest Texas: implications of smectite diagenesis on sandstone cementation: Journal of Sedimentary Petrology, v. 49, p. 55-70.

Bouchez, J., Gaillardet, J., France-Lanord, C., Maurice, L., and Dutra-Maia, P., 2011, Grain size control of river suspended sediment geochemistry: clues from Amazon River depth profiles: Geochemistry, Geophysics, Geosystems, v. 12, doi: 10.1029/2010GC003380.

Buggle, B., Glaser, B., Hambach, U., Gerasimenko, N., and Marković, S., 2011, An evaluation of geochemical weathering indices in loess-paleosol studies.: Quaternary International, v. 240, p. 12-21.

Burke, B.C., Heimsath, A.M., and White, A.F., 2007, Coupling chemical weathering with soil production across soil-mantled landscapes: Earth Surface Processes and Landforms, v. 32, p. 853-873.

Burke, B.C., Heimsath, A.M., Dixon, J.L., Chappell, J., and Yoo, K., 2009, Weathering the escarpment: chemical and physical rates and process, south-eastern Australia: Earth Surface Processes and Landforms, v. 34, p. 768-785.

Cawood, P.A., Hawkesworth, C.J., and Dhuime, B., 2012, Detrital zircon record and tectonic setting: Geology, v. 40, p. 875-878.

Chen, B., Joachimski, M. M., Shen, S., Lambert, L. L., Lai, X., Wang, X., Chen, J., and Yuan, D., 2013, Permian ice volume and palaeoclimate history: oxygen isotope proxies revisited: Gondwana Research v. 24, p. 77-89.

Chetelat, B., Liu, C.-Q., Wang, Q., and Zhang, G., 2013, Assessing the influence of lithology on weathering indices of Changjiang river sediments: Chemical Geology, v. 359, p. 108-115.

Clift, P.D., Wan, S., and Blusztajn, J., 2014, Reconstructing chemical weathering, physical erosion and monsoon intensity since 25 Ma in the northern South China Sea: a review of competing proxies: Earth-Science Reviews, v. 130, p. 86-102.

Cox, R., Lowe, D.R., and Cullers, R.L., 1995, The influence of sediment recycling and basement composition on evolution of mudrock chemistry in the southwestern United States: Geochimica et Cosmochimica Acta, v. 59, p. 2919-2940.

Cullers, R.L., 2000, The geochemistry of shales, siltstones and sandstones of Pennsylvanian-Permian age, Colorado, USA: implications for provenance and metamorphic studies: Lithos, v. 51, p. 181-203.

Cullers, R.L., Basu, A., and Suttner, L.J., 1988, Geochemical signature of provenance in sand-size material in soil and stream sediments near the Tobacco Root batholith, Montana, U. S. A.: Chemical Geology, v. 70, p. 335-348.

Ding, Z., Sun, J., Rutter, N. W., Rokosh, D., and Liu, T., 1999, Changes in sand content of loess deposits along a north-south transect of the Chinese Loess Plateau and the implications for desert variations:

Quaternary Research, v. 52, p. 56-62.
Ding, Z., Sun, J., Yang, S., and Liu, T. S., 2001, Geochemistry of the Pliocene red clay formation in the Chinese Loess Plateau and implications for its origin, source provenance and paleoclimate change: Geochimica et Cosmochimica Acta, v. 65, p. 901-913.
DiMichele, W. A., Montañez, I. P., Poulsen, C. J., and Tabor, N. J., 2009, Climate and vegetational regime shifts in the late Paleozoic ice age earth: Geobiology, v. 7, p. 200-226.
Dixon, J.L., Hartshorn, A.S., Heimsath, A.M., Dibiase, R.A., and Whipple, K.X., 2012, Chemcial weathering response to tectonic forcing: a soils perspective from the San Gabriel Mountains, California: Earth and Planetary Science Letters, v. 323-324, p. 40-49.
Embelton, B.J.J., McElhinny, M.W., Ma, X., Zhang, Z., and Li, Z., 1996, Permo-Triassic magnetostratigraphy in China: the type section near Taiyuan, Shanxi Province, North China: Geophysical Journal International, v. 126, p. 382-388.
Fedo, C.M., Nesbitt, H.W., and Young, G.M., 1995, Unraveling the effects of potassium metasomatism in sedimentary rocks and paleosols, with implications for paleoweathering conditions and provenance: Geology, v. 23, p. 921-924.
Fedo, C.M., Young, G.M., and Nesbitt, H.W., 1997a, Paleoclimatic control on the composition of the Paleoproterozoic Serpent Formation, Huronian Supergroup, Canada: a greenhouse to icehouse transition: Precambrian Research, v. 86, p. 201-223.
Fedo, C.M., Young, G.M., Nesbitt, H.W., and Hanchar, J.M., 1997b, Potassic and sodic metasomatism in the Southern Province of the Canadian Shield: evidence from the Paleoproterozoic Serpent Formation, Huronian Supergroup, Canada: Precambrian Research, v. 84, p. 17-36.
Feng, B., 2012, Study on coal-accumulating characteristic of Shanxi Formation and low Shihezi Formation in Yongcheng Coalfield, Henna Province: Journal of Henan Polytechnic University (Natural Science) v. 31, p. 177-181 (in Chinese with English abstract).
Fielding, C.R., Frank, T.D., Birgenheier, L.P., Rygel, M.C., Jones, A.T., and Roberts, J., 2008, Stratigraphic imprint of the Late Paleozoic Ice Age in eastern Australia: a record of alternating glacial and nonglacial climate regime: Journal of the Geological Society, v. 165, p. 129-140.
Gaillardet, J., Dupré, B., and Allègre, C.J., 1999, Geochemistry of large river suspended sediments: silicate weathering or recycling tracer?: Geochimica et Cosmochimica Acta, v. 63, p. 4037-4051.
Gao, S., Luo, T., Zhang, B., Zhang, H., Han, Y., Zhao, Z., and Hu, Y., 1998, Chemical composition of the continental crust as revealed by studies in East China: Geochimica et Cosmochimica Acta, v. 62, p. 1959-1975.
Garzanti, E., Padoan, M., Setti, M., Najman, Y., Peruta, L., and Villa, I.M., 2013, Weathering geochemistry and Sr-Nd fingerprints of equatorial upper Nile and Congo muds: Geochemistry Geophysics Geosystems, v. 14, p. 292-316.
Garzanti, E., Padoan, M., Setti, M., López-Galindo, A., and Villa, I.M., 2014, Provenance versus weathering control on the composition of tropical river mud (southern Africa): Chemical Geology, v. 366, p. 61-74.
Gradstein, F.M., Ogg, J.G., Schmitz, M.D., and Ogg, G.M., 2012, The geological time scale 2012: Oxford, Elsevier, 1144 p.
Han, J. Lu, H., Wu, N., and Guo, Z., 1996, The magnetic susceptibility of modern soils in China and its use for paleoclimate reconstruction: Studia Geophysica et Geodaetica, v. 40, p. 262-275.
Harnois, L., 1988, The CIW index: a new chemical index of weathering: Sedimentary Geology, v. 55, p. 319-322.

560 Hilton, J., and Cleal, C.J., 2007, The relationship between Euramerican and Cathaysian tropical floras in
561 the Late Palaeozoic: palaeobiogeographical and palaeogeographical implications: Earth-Science
562 Reviews, v. 85, p. 85-116.
563 Huang, B., Otofuji, Y.-i., Zhu, R., Shi, R., and Wang, Y., 2001, Paleomagnetism of Carboniferous
564 sediments in the Hexi corridor: its origin and tectonic implications: Earth and Planetary Science
565 Letters, v. 194, p. 135-149.
566 Isbell, J.L., Henry, L.C., Gulbranson, E.L., Limarino, C.O., Fraiser, M.L., Koch, Z.J., Ciccioli, P.L., and
567 Dineen, A.A., 2012, Glacial paradoxes during the late Paleozoic ice age: evaluating the equilibrium
568 line altitude as a control on glaciation: Gondwana Research, v. 22, p. 1-19.
569 Jacobson, A.D., Blum, J.D., Chamberlain, C.P., Craw, D., and Koons, P.O., 2003, Climatic and tectonic
570 controls on chemical weathering in the New Zealand Southern Alps: Geochimica et Cosmochimica
571 Acta, v. 67, p. 29-46.
572 Johnsson, M.J., 1993, The system controlling the composition of clastic sediments, *in* Johnsson, M.J., and
573 Basu, A., eds., Processes controlling the composition of clastic sediments: Geological Society of
574 America Special Papers, v. 284, p. 1-20.
575 Kamei, A., Fukushi, K., Takagi, T., and Tsukamoto, H., 2012, Chemical overprinting of magmatism by
576 weathering: a practical method for evaluating the degree of chemical weathering of granitoids: Applied
577 Geochemistry, v. 27, p. 796-805.
578 Khomo, L., 2008, Weathering and soil properties on old granitic catenas along climo-topographic gradients
579 in Kruger National Park [Ph.D. thesis]: Johannesburg, University of the Witwatersrand, 224 p.
580 Land, L.S., Mack, L.E., Milliken, K.L., and Lynch, L., 1997, Burial diagenesis of argillaceous sediment,
581 south Texas Gulf of Mexico sedimentary basin: a reexamination: Geological Society of America
582 Bulletin, v. 109, p. 2-15.
583 Lupker, M., France-Lanord, C., Galy, V., Lavé, J., and Kudrass, H., 2013, Increasing chemical weathering
584 in the Himalayan system since the Last Glacial Maximum: Earth and Planetary Science Letter, v. 365,
585 p. 243-252.
586 McLennan, S.M., 1993, Weathering and global denudation: The Journal of Geology, v. 101, p. 295-303.
587 McLennan, S.M., Heming, S., McDaniel, D.K. and Hanson, G.N., 1993, Geochemical approaches to
588 sedimentation, provenance, and tectonics, *in* Johnsson, M.J., and Basu, A., eds., Processes controlling
589 the composition of clastic rocks: Geological Society of America Special Paper 284, p. 21-40.
590 Meunier, A., Caner, L., Hubert, F., Albani, A.E., and Prêt, D., 2013, The weathering intensity scale (WIS):
591 an alternative approach of the chemical index of alteration (CIA): American Journal of Science, v. 313,
592 p. 113-143.
593 Montañez, I.P., Tabor, N.J., Niemeier, D., DiMichele, W.A., Frank, T.D., Fielding, C.R., Isbell, J.L.,
594 Birgenheier, L.P., and Rygel, M.C., 2007, $CO_2$-forced climate and vegetation instability during Late
595 Paleozoic deglaciation: Science, v. 315, p. 87-91.
596 Montañez, I. P., and Poulsen, C. J., 2013, The late Paleozoic Ice Age: an evolving paradigm: The Annual
597 Review of Earth and Planetary Sciences, v. 41, p. 629-656.
598 Morey, G.B., and Setterholm, D.R., 1997, Rare earth elements in weathering profiles and sediments of
599 Minnesota: implications for provenance studies: Journal of Sedimentary Research, v. 67, p. 105-115.
600 Nesbitt, H.W., Fedo, C.M., and Young, G.M., 1997, Quartz and feldspar stability, steady and
601 non-steady-state weathering, and petrogenesis of siliciclastic sands and mud: The Journal of Geology,
602 v. 105, p. 173-191.
603 Nesbitt, H.W., and Markovics, G., 1997, Weathering of granodioritic crust, long-term storage of elements

604 in weathering profiles, and petrogenesis of siliciclastic sediments: Geochimica et Cosmochimica Acta,
605 v. 61, p. 1653-1670.
606 Nesbitt, H.W., Markovics, G., and Price, R.C., 1980, Chemical processes affecting alkalis and alkaline
607 earths during continental weathering: Geochimica et Cosmochimica Acta, v.44, p. 1659-1666.
608 Nesbitt, H.W., and Young, G.M., 1982, Early Proterozoic climates and plate motions inferred from major
609 element chemistry of lutites: Nature, v. 299, p. 715-717.
610 Nesbitt, H.W., and Young, G.M., 1984, Prediction of some weathering trends of plutonic and volcanic
611 rocks based on thermodynamic and kinetic considerations: Geochimica et Cosmochimica Acta, v. 48, p.
612 1523-1534.
613 Nesbitt, H.W., and Young, G.M., 1996, Petrogenesis of sediments in the absence of chemical weathering:
614 effects of abrasion and sorting on bulk composition and mineralogy: Sedimentology, v. 43, p. 341-358.
615 Nesbitt, H.W., Young, G.M., Mclennan, S.M., and Keays, R.R., 1996, Effects of chemical weathering and
616 sorting on the petrogenesis of siliciclastic sediments, with implications for provenance studies: The
617 Journal of Geology, v. 104, p. 525-542.
618 Parker, A., 1970, An index of weathering for silicate rocks: Geological Magazine, v. 107, p. 501-504.
619 Poulsen, C.J., Pollard, D., Montañez, I. P., and Rowley, D., 2007, Late Paleozoic tropical climate response
620 to Gondwanan deglaciation: Geology, v. 35, p. 771-774.
621 Price, J.R., and Velbel, M.A., 2003, Chemical weathering indices applied to weathering profiles developed
622 on heterogeneous felsic metamorphic parent rocks: Chemical Geology, v. 202, p. 397-416.
623 Rasmussen, C., Brantley, S., Richter, D., Blum, A., Dixon, J., and White, A.F., 2011, Strong climate and
624 tectonic control on plagioclase weathering in granitic terrain: Earth and Planetary Science Letters, v.
625 301, p. 521-530.
626 Reiche, P., 1943, Graphic representation of chemical weathering: Journal of Sedimentary Petrology, v. 13,
627 p. 58-68.
628 Riebe, C.S., Kirchner, J.W., and Finkel, R.C., 2004, Erosional and climatic effects on long-term chemical
629 weathering rates in granitic landscapes spanning diverse climate regimes: Earth and Planetary Science
630 Letters, v. 224, p. 547-562.
631 Riebe, C.S., Kirchner, J.W., Granger, D.E., and Finkel, R.C., 2001, Strong tectonic and weak climatic
632 control of long-term chemical weathering rates: Geology, v. 29, p. 511-514.
633 Rieu, R., Allen, P.A., Plötze, M., and Pettke, T., 2007, Climatic cycles during a Neoproterozoic "snowball"
634 glacial epoch: Geology, v. 35, p. 299-302.
635 Rudnick, R., and Gao, S., 2003, Composition of the continental crust, *in* Rudnick, R.L., ED., Treatise on
636 Geochemistry: Amsterdam, Elsevier, v., 3, p. 1-64.
637 Ruxton, B.P., 1968, Measures of the degree of chemical weathering of rocks, The Journal of Geology, v. 76,
638 p. 518-527.
639 Schatz, A.-K., Scholten, T., and Kühn, P., 2015, Paleoclimate and weathering of the Tokaj (Hungary)
640 loess-paleosol sequence. Paleogeography, Paleoclimatology, Palaeoecology, v. 426, p. 170-182.
641 Scheffler, K., Hoernes, S., and Schwark, L., 2003, Global changes during Carboniferous-Permian
642 glaciation of Gondwana: linking polar and equatorial climate evolution by geochemical proxies:
643 Geology, v. 31: p. 605-608.
644 Singh, P., and Rajamani, V., 2001, REE geochemistry of recent clastic sediments from the Kaveri
645 floodplains, southern India: implication to source area weathering and sedimentary processes:
646 Geochimica et Cosmochimica Acta, v. 65, p. 3093-3108.
647 Soreghan, G. S., Soreghan, M. J., Poulsen, C. J., Young, R. A., Eble, C. F., Sweet, D. E., and Davogustto, O.

C., 2008, Anomalous cold in the Pangaean tropics: Geology, v. 36, p. 659-662.
Soreghan, G. S., Sweeet, D. E., and Heavens, N. G., 2014a, Upland glaciation in Tropical Pangaea: geologic evidence and implications for late Paleozoic climate modeling: The Journal of Geology, v. 122, p. 137-163.
Soreghan, M. J., Heavens, N., Soreghan, G. S., Link, P. K., and Hamilton, M. A., 2014b, Abrupt and high-magnitude changes in atmospheric circulation recorded in the Permian Maroon Formation, tropical Pangaea: Geological Society of America Bulletin, v. 126, p. 569-584.
Soreghan, M. J., and Soreghan, G. S. L., 2007, Whole-rock geochemistry of upper Paleozoic loessite, western Pangaea: implications for paleo-atmospheric circulation: Earth and Planetary Science Letters, v. 255, p. 117-132.
Tabor, N. J., 2007, Permo-Pennsylvanian paleotemperatures from Fe-oxide and phyllosilicate $\delta^{18}O$ values: Earth and Planetary Science Letters, v. 253, p. 159-171.
Tabor, N. J., Montanez, I. P., Scotese, C. R., Poulsen, C. J., and Mack, G. H., 2008, Paleosol archives of environmental and climatic history in paleotropical western Pangea during the latest Pennsylvanian through Early Permian, *in* Fielding, C. R., Frank, T. D., and Isbell, J. I. ed., Resolving the Late Paleozoic Ice Age in time and space: Geological Society of America Special Paper 441, p. 291-303.
Tabor, N. J., and Poulsen, C. J., 2008, Paleoclimate across the late Pennsylvanian-Early Permian tropical palaeolatitudes: a review of climate indicators, their distribution, and relation to palaeophysiographic climate factors: Palaeogeography, Palaeoclimatology, Palaeoecology, v. 268, p. 293-310.
Taylor, J.R., 1997, An introduction to error analysis: the study of uncertainties in physical measurements: Sausalito, California, University Science Books, 1-327pp.
Taylor, S.R., and McLennan, S.M., 1985, The continental crust: Its composition and evolution: Oxford, Blackwell, 1-312 pp.
Torsvik, T.H., and Cocks, L.R.M., 2004, Earth geography from 400 to 250 Ma: a paleomagnetic, faunal and facies review: Journal of the Geological Society, v. 161, p. 555-572.
Wang, H., 1985, Atlas of the palaeogeography of China: Beijing, Cartographic Publishing House, p. 74-80.
Wang, H., and Mo, X., 1995, An outline of the tectonic evolution of China: Episodes, v. 18, p. 6-16.
Wang, J., 2010, Late Paleozoic macrofloral assemblage from Weibei Coalfield, with reference to vegetational change through the late Paleozoic ice age in the North China Block: International Journal of Coal Geology, v. 83, p. 292-317.
Wang, J., and Pfefferkorn, H. W., 2013, The Carboniferous-Permian transition on the North China microcontinent-oceanic climate in the tropics: International Journal of Coal Geology, v. 119, p. 106-113.
Wang, R., 1982, Permian System of East Henan: Journal of China University of Mining and Technology, v. 2, p. 50-60 (in Chinese with English abstract).
Wang, Y., Zhou, L., Zhao, L., Ji, M., and Gao, H., 2010, Paleozoic uplands and unconformity in the North China Block: constraints from zircon LA-ICP-MS dating and geochemical analysis of bauxite: Terra Nova, v. 22, p. 264-273.
Wang, Z., and Zhang, W., 1985, Discovery of conodonts in the upper Taiyuan Formation in Yuxian, Henan: Journal of Stratigraphy, v. 9, p. 228-230 (in Chinese with English Abstract).
West, A.J., Galy, A., and Bickle, M., 2005, Tectonic and climatic controls on silicate weathering: Earth and Planetary Science Letters, v. 235, p. 211-228.
White, A.F., Bullen, T.D., Schulz, M.S., Blum, A.E., Huntington, T.G., and Peters, N.E., 2001, Differential rates of feldspar weathering in granitic regoliths: Geochimica et Cosmochimica Acta, v. 65, p.

847-869.
White, A.F., and Blum, A.E., 1995, Effects of climate on chemical weathering in watersheds: Geochimica et Cosmochimica Acta, v. 59, p. 1729-1747.
Wilkinson, B.H., 2005, Humans as geological agents: a deep-time perspective: Geology, v. 33, p. 161-164.
Wilson, M.J., 2004, Weathering of the primary rock-forming minerals: processes, products and rates: Clay Minerals, v. 39, p. 233-266.
Xiao, S., Liu, W., Li, A., Yang, S., and Lai, Z., 2010, Pervasive autocorrelation of the chemical index of alteration in sedimentary profiles and its palaeoenvironmental implications: Sedimentology, v. 57, p. 670-676.
Yan, D., Chen, D., Wang, Q., and Wang, J., 2010, Large-scale climatic fluctuations in the latest Ordovician on the Yangtze block, south China: Geology, v. 38, p. 599-602.
Yang, J., Cawood, P.A., Du, Y., Feng, B., and Yan, J., 2014, Global continental weathering trends across the Early Permian glacial to postglacial transition: correlating high- and low-paleolatitude sedimentary records: Geology, v. 42, p. 835-838.
Yang, J., Du, Y., Cawood, P.A., and Xu, Y., 2012a, Modal and geochemical compositions of the Lower Silurian clastic rocks in North Qilian, NW China: implications for provenance, chemical weathering, and tectonic setting: Journal of Sedimentary Research, v. 82, p. 92-103.
Yang, J., Du, Y., Cawood, P.A., and Xu, Y., 2012b, From subduction to collision in the Northern Tibetan Plateau: evidence from the Early Silurian clastic rocks, Northwestern China: The Journal of Geology, v. 120, p. 49-67.
Yang, S., Ding, F., and Ding, Z., 2006, Pleistocene chemical weathering history of Asian arid and semi-arid regions recorded in loess deposits of China and Tajikistan: Geochimica et Cosmochimica Acta, v. 70, p. 1695-1709.
Young, G.M., Minter, W.E.L., and Theron, J.N., 2004, Geochemistry and palaeogeography of upper Ordovician glaciogenic sedimentary in the Table Mountain Group, South Africa: Palaeogeography, Palaeoclimatology, Palaeoecology, v. 214, p. 323-345.
Young, G.M., and Nesbitt, H.W., 1999, Paleoclimatology and provenance of the glaciogenic Gowganda Formation (Paleoproterozoic), Ontario, Canada: a chemostratigraphic approach: GSA Bulletin, v. 111, p. 264-274.
Zhang, H., 1999, Control of palaeoclimatic change on late Palaeozoic coal accumulation of the North China plate: Acta Geologica Sinica, v. 73, p. 131-139 (in Chinese with English abstract).
Zhang, S., 1990, Paleontology of the coal-bearing late Paleozoic strata in Dengfeng, Henan: Journal of Stratigraphy, v. 14, p. 140-144 (in Chinese with English abstract).
Zhu, H., Yang, G., and Sheng, A., 1996, A study on palaeomagnetism of Permian strata in the Dafengkou section, Yuzhou, Henan Province: Acta Geologica Sinica, v. 70, p. 121-128 (in Chinese with English abstract).

**Figure Captions:**

Figure 1. Early Permian global paleogeographic reconstruction (Huang et al., 2001; Torsvik and Cocks, 2004) showing the positions of western Colorado and north-central Texas in southern North America of west tropical Pangea and of Yongcheng Coalfield in North China. North China is separated from the Pangea by the Tethys Ocean to the west and by Panthalassic Ocean to the east.

Figure 2. A. Generalized tectonic map of China showing the position of Henan Province. B.

Map of Henan Province showing the positions of sampled core sections in the Yongcheng Coalfield with the simplified stratigraphy in the insert. Samples are collected from the Lower Permian sedimentary sequences of core Zk1401 (C) and core Zk0901 (D). Zircon age data is from Yang et al. (2014).

Figure 3. Stratigraphic variations of mineral composition and values of representative weathering indices for mudstone and siltstone samples of core Zk1401 (A) and Zk0901 (B). CaO* in index calculation indicates carbonate- and phosphate-corrected CaO (McLennan, 1993). Abbreviations: Qz: quartz, Cl: chlorite, Il: illite, Ka: kaolinite, F: feldspar, Cc: calcite and Sd: siderite. For weathering index values, core samples of Zk1401 and Zk0901 are marked in green and red symbols, respectively and filled circles and diamonds denote the samples with high siderite and chlorite contents, respectively. In B, X.F. is short for Xiashihezi Formation.

Figure 4. Correlation diagrams of CIA with other weathering indices for studied samples and inferred average source composition, the upper crust of southern North China (SNC, Gao et al., 1998). Statistical results ($r^2$ and P value) and regression lines are shown. In CIA-$\tau_{Na}$ plot (D) the average loessites of Maroon Formation in west Pangea (Soreghan et al., 2014b), average loess L1-5 of Chinese Loess Plateau (Ding et al., 2001), average upper continental crust (UCC, Taylor and McLennan, 1985) and average upper crust of interior North China carton (INC, Gao et al., 1998) are also shown. For the average loessites of Maroon Formation in west Pangea (Soreghan et al., 2014b), the $\tau_{Na}$ value was calculated based on three UCC composition models proposed by Taylor and McLennan (1985), Condie (1993) and Rudnick and Gao (2003), marked by filled square, blank square and blank triangle.

Figure 5. Plots of A-CN-K (A), $M^+$-4Si-$R^{2+}$ (B), AF-CNK-M (C), and $R^{3+}/(R^{3+}+R^{2+}+M^+)$-$\Delta$4Si% (D) for sedimentary rock samples from cores Zk1401 and Zk0901 showing chemical weathering trend of the average upper crust of southern North China carton (SNC, Gao et al., 1998) and possible diagenetic influences. Also shown are average upper continental crust (UCC, Taylor and McLennan, 1985) and average upper crust of interior North China craton (INC, Gao et al., 1998) on A-CN-K diagram for comparison. Abbreviations: A: $Al_2O_3$, CN: CaO*+$Na_2O$, CNK: CaO*+$Na_2O$+$K_2O$, K: $K_2O$, AF: $Al_2O_3$+$FeO_{3(T)}$, and M: MgO. Sample symbols are the same as in Figure 4.

Figure 6. Plots of quartz/clay mineral ratio vs. Al/Si ratio (A), WIP (B), LCWP (C) and $\tau_{Na}$ (D) showing no significant sedimentary sorting effect on sample compositions. Regression line for Zk1401 samples are also shown in A and B. In B, four samples (shaded areas) are not included in correlation analysis. Sample symbols are the same as in Figure 4.

Figure 7. A. Distribution of compiled modern granitic landscape soil sites on global map, where some sites are too close to be shown separately and the number of sites represented by one circle are marked, and B. Plot of modern surface chemical weathering data from these granitic landscapes documenting controls of physical erosion rate (E), mean annual temperature (MAT) and mean annual precipitation (MAP) on land surface soil weathering intensity indexed by $\tau_{Na}$. A linear relationship between surface soil $\tau_{Na}$ and MAT was observed for sites with E < 100 m/Ma and MAP > 400 mm/a, and developed into a $\tau_{Na}$-MAT transfer function. One site with very low physical erosion rate (< 2 m/Ma) and three sites with high MAP (~4000 mm/a), but cool temperatures (~8 °C) were not

included. Average $\tau_{Na}$ values of the Asselian-Sakmarian sediments of Shanxi Formation in North China and Maroon Formation (using UCC composition model of Taylor and McLennan (1985)) in west Colorado of west tropical Pangea were shown for comparison. Also shown is the $\tau_{Na}$ value of the average loess L1-5 in Chinese Loess Plateau. The standard error (S.E.) is calculated as:

$$\text{S.E.} = \sqrt{\sum \sigma^2 / n}$$

, where $\sum\sigma^2$ is the sum of squares of deviation of measured MAT from linear model based MAT and n is the number of the weathering sites used for this linear model.

Figure 1



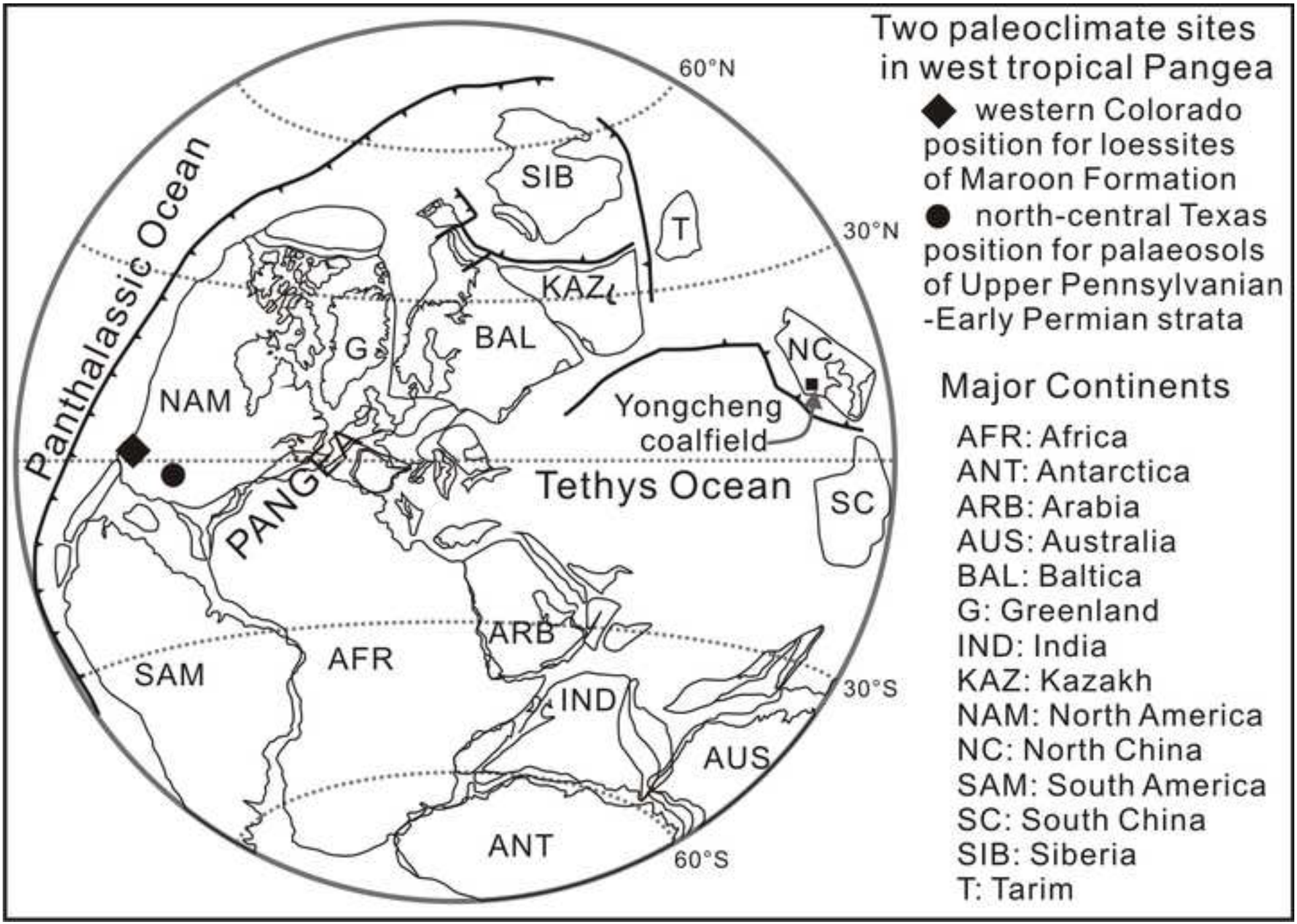

Figure 2

Click here to download Figure P11-Figure-2.TIF

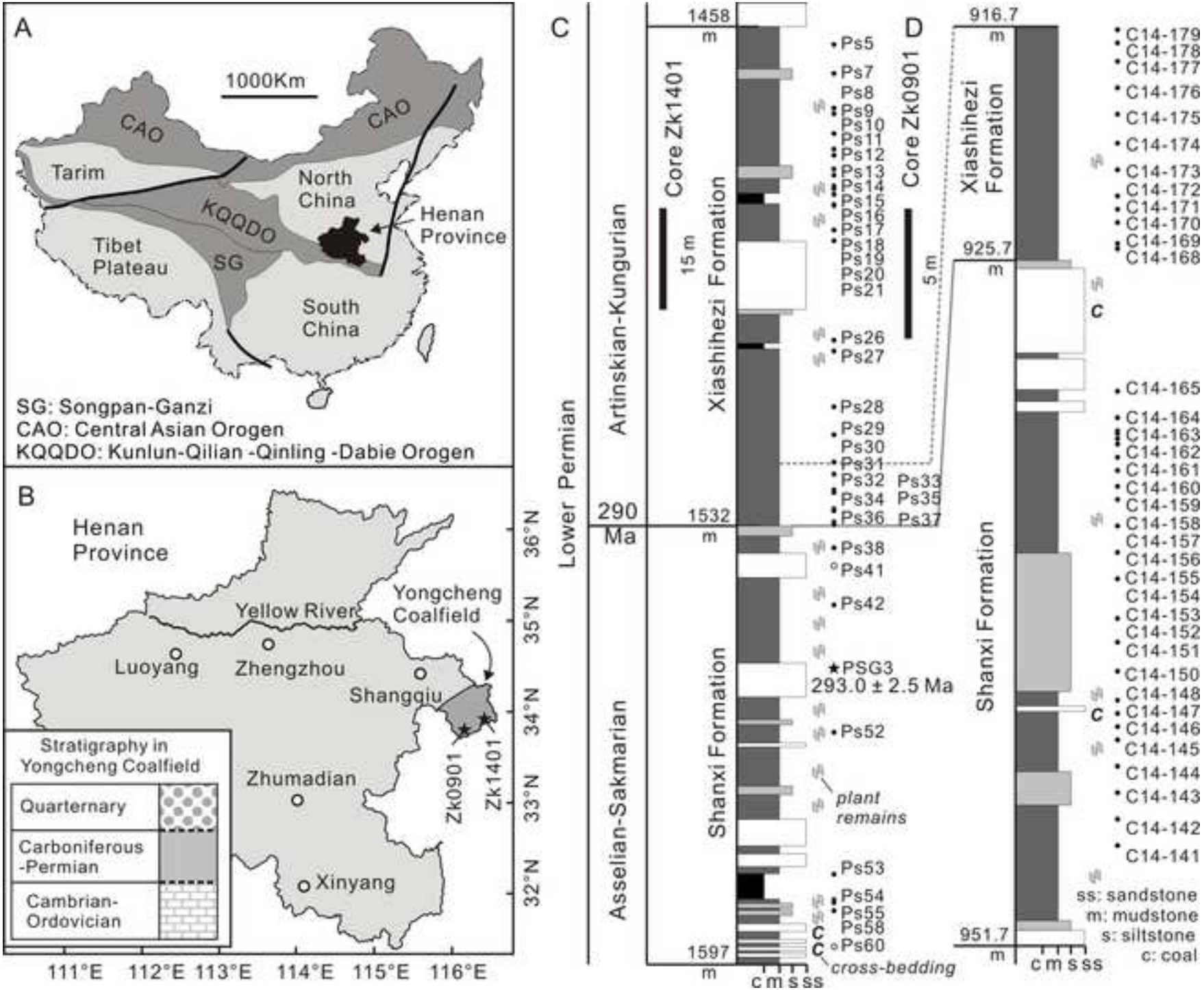

Figure 3

Click here to download Figure P11-Figure-3.TIF

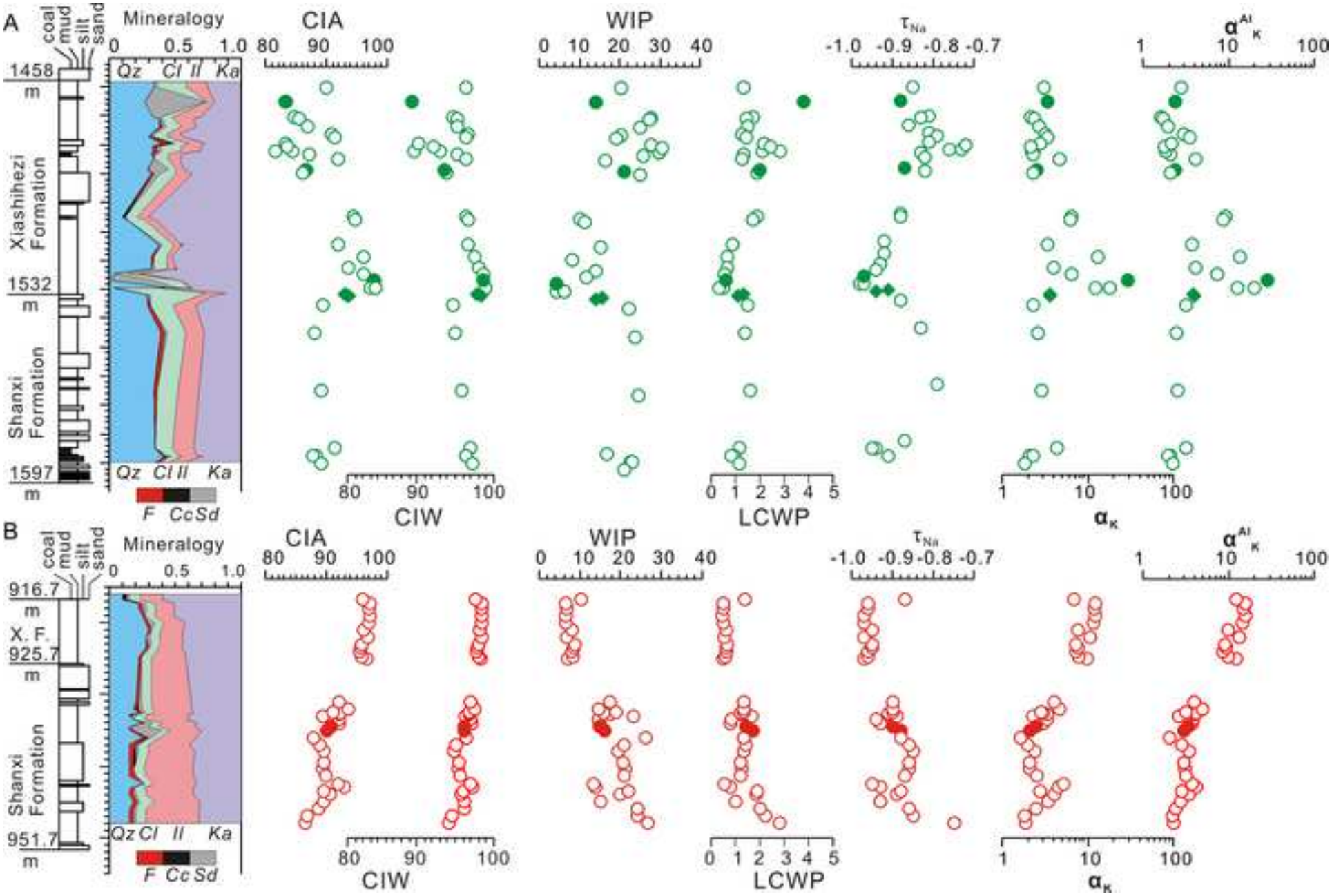

Figure 4

Click here to download Figure P11-Figure-4.TIF

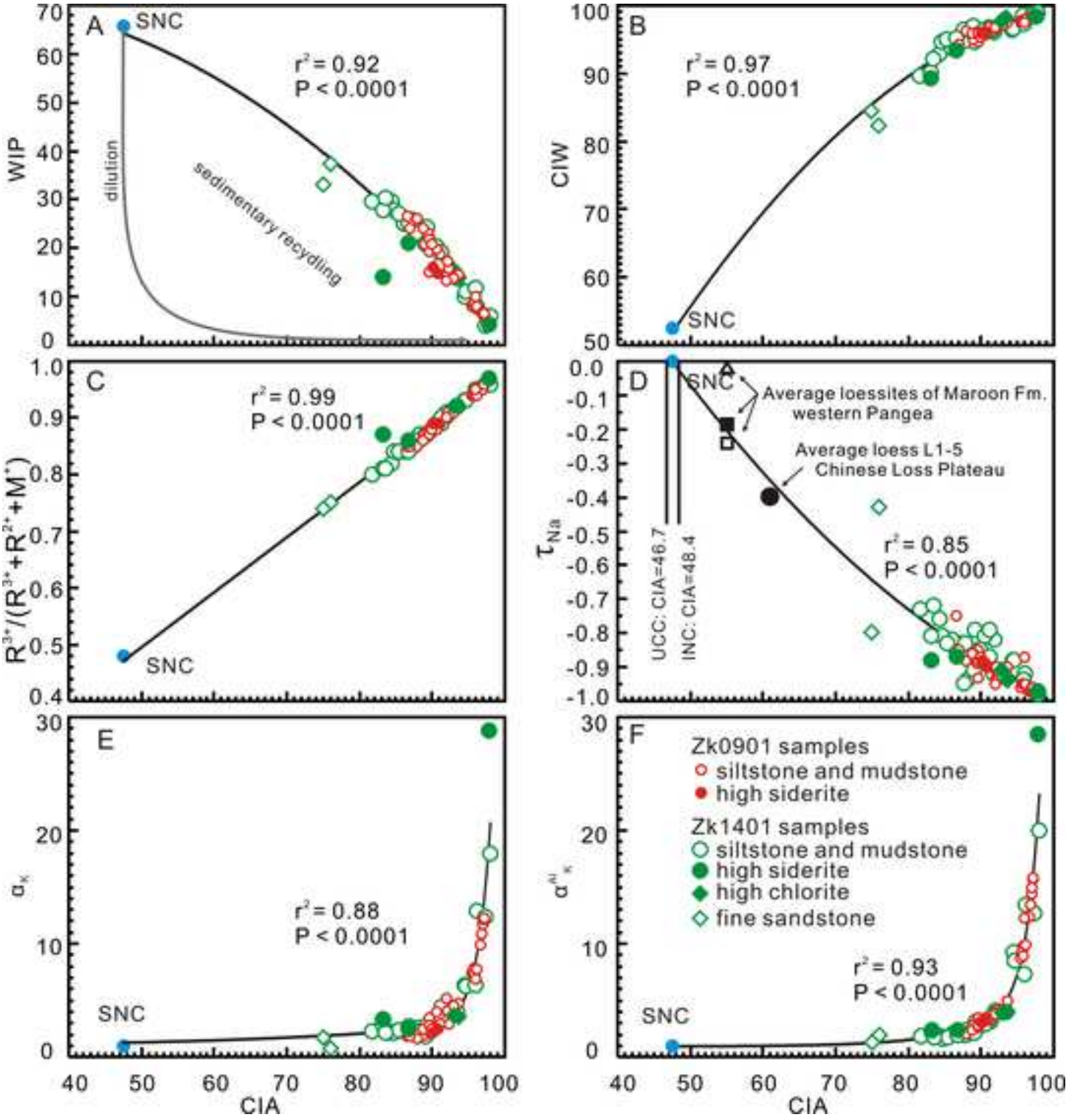

Figure 5

Click here to download Figure P11-Figure-5.TIF

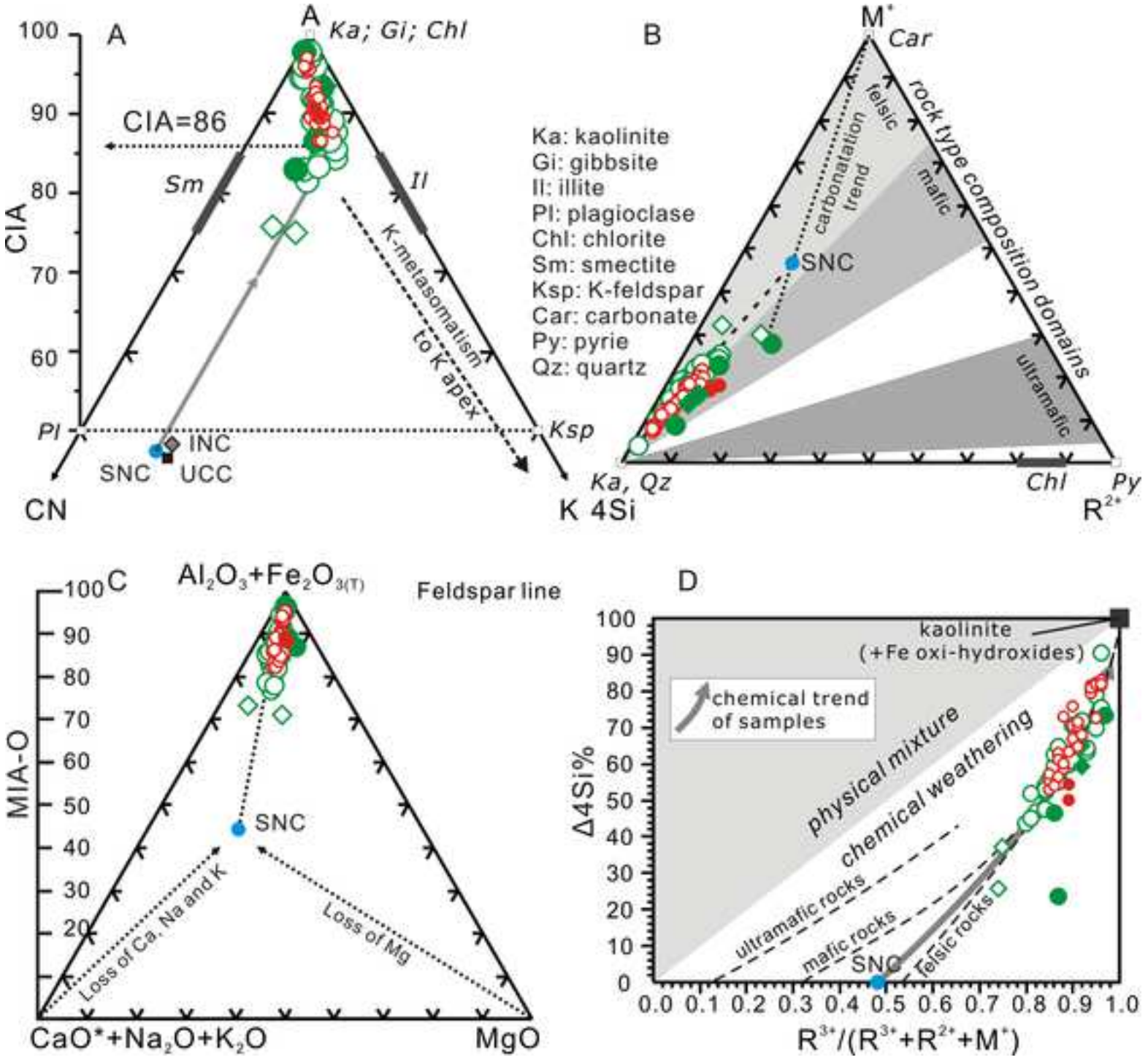

Figure 6



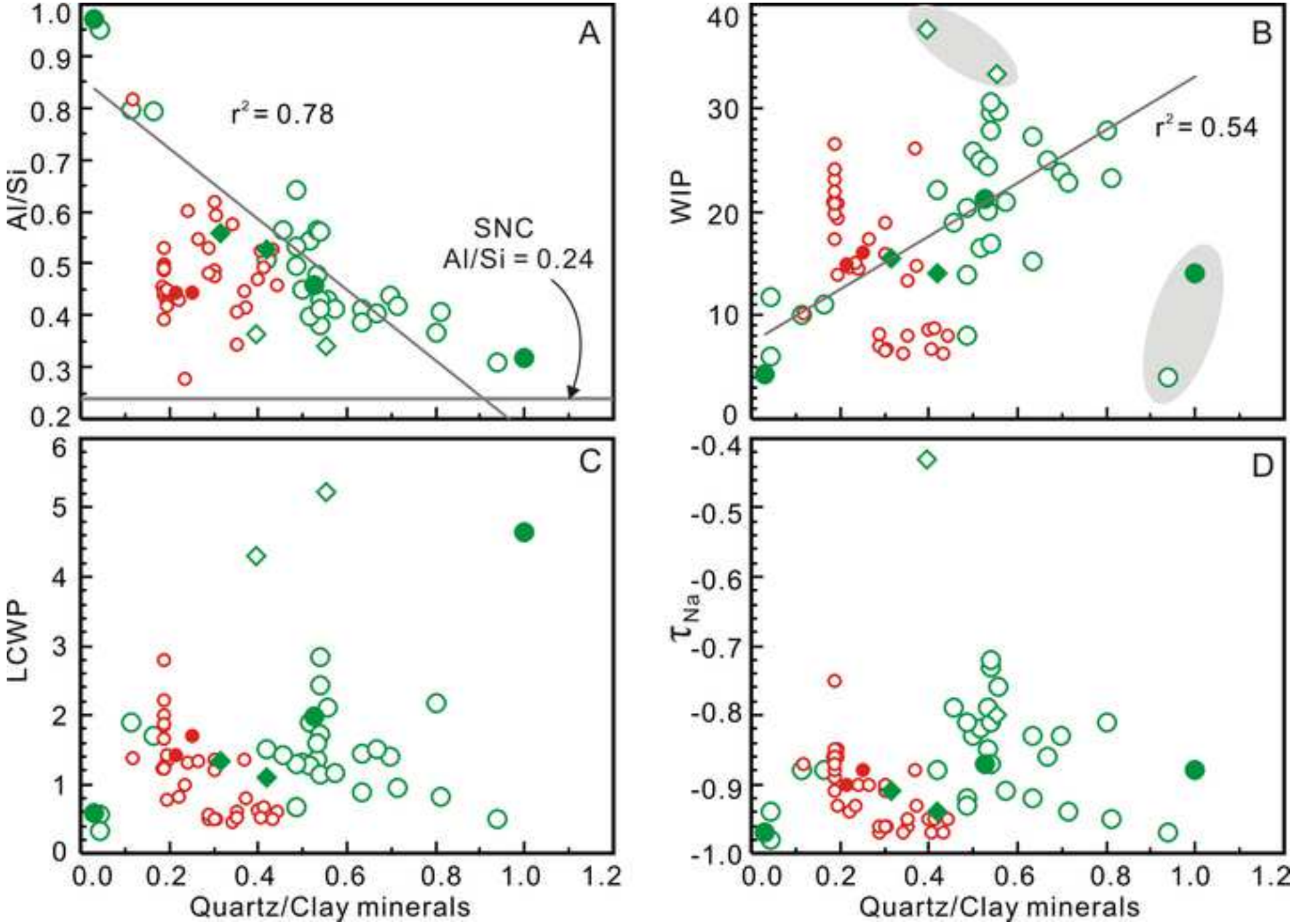

Figure 7



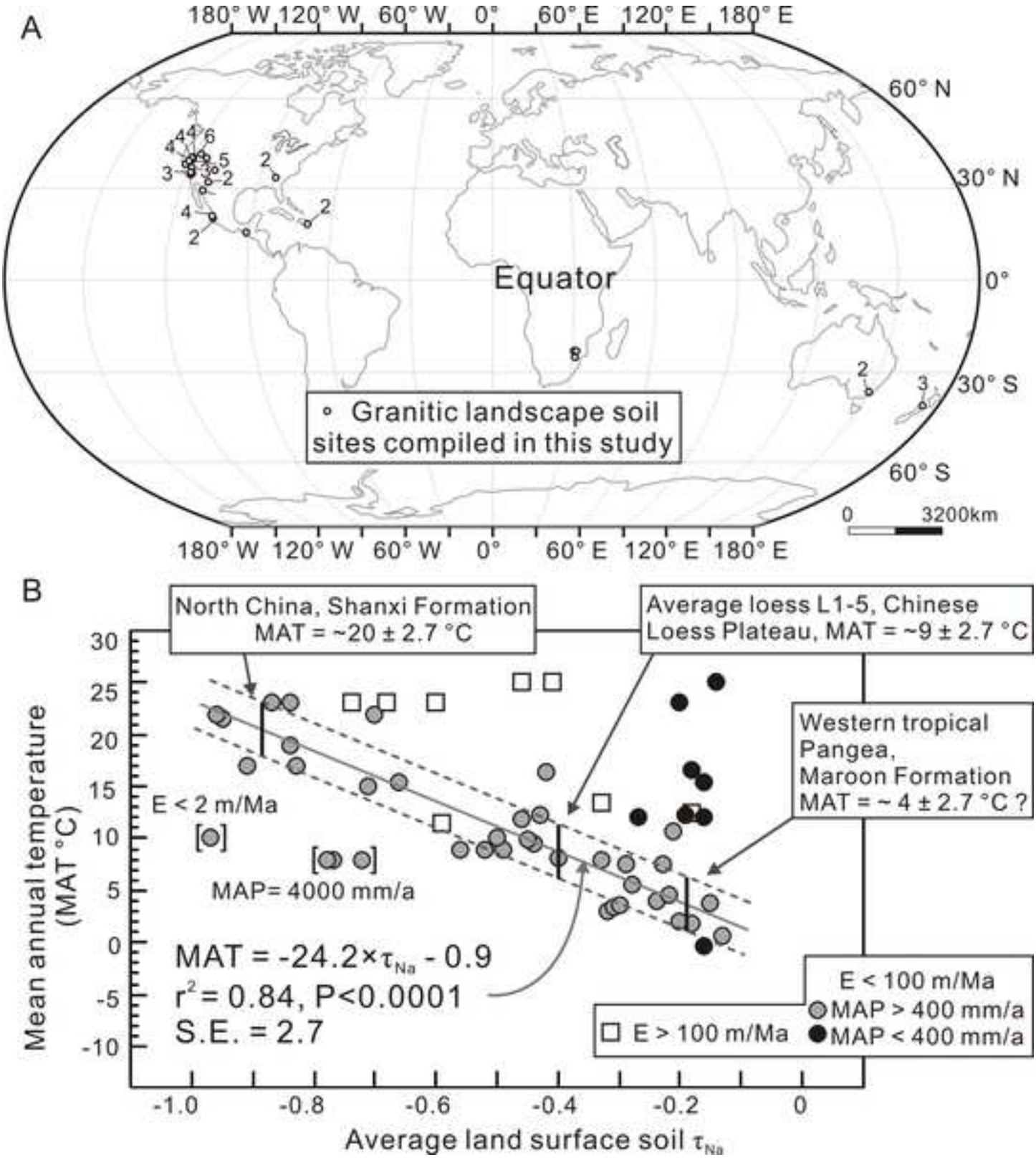

Table 1

Table 1 Chemical weathering indices and their computational formula

| Weathering indices compiled | | Equation for index calculation | Note* | Sources |
|---|---|---|---|---|
| weathering index of Parker | | $WIP = 100\times[(2Na_2O/0.35)+(MgO/0.9)+(2K_2O/0.25)+(CaO^*/0.7)]$ | molar | Parker, 1970 |
| indices based on feldspar weathering | | $CIA = 100\times Al_2O_3/(Al_2O_3+CaO^*+Na_2O+CaO+K_2O)$ | molar | Nesbitt and Young, 1982 |
| chemical index of weathering, CIW | | $CIW = 100\times Al_2O_3/(Al_2O_3+CaO^*+Na_2O)$ | molar | Harnois, 1988 |
| plagioclase index of alteration, PIA | | $PIA = 100\times(Al_2O_3-K_2O)/(Al_2O_3+CaO^*+Na_2O+CaO-K_2O)$ | molar | Fedo et al., 1995 |
| chemical proxy of alteration, CPA | | $CPA = 100\times(Al_2O_3)/(Al_2O_3+Na_2O)$ | molar | Cullers, 2000; Buggle et al., 2011 |
| modified chemical index of alteration | | $CIX = 100\times(Al_2O_3)/(Al_2O_3+Na_2O+K_2O)$ | molar | Garzanti et al., 2014 |
| elemental weathering indices, $\alpha_E$ and $\alpha^{Al}_E$ | | $\alpha_{Na} = [Sm/Na]_{sediment}/[Sm/Na]_{source\ rock}$ | mass | Gaillardet et al., 1999 |
| | | $\alpha_{Ca} = [Ti/Ca]_{sediment}/[Ti/Ca]_{source\ rock}$ | mass | |
| | | $\alpha_{Mg} = [Al/Mg]_{sediment}/[Al/Mg]_{source\ rock}$ | mass | |
| | | $\alpha_{K} = [Th/K]_{sediment}/[Th/K]_{source\ rock}$ | mass | |
| | | $\alpha_{Sr} = [Nd/Sr]_{sediment}/[Nb/Sr]_{source\ rock}$ | mass | |
| | | $\alpha_{Ba} = [Th/Ba]_{sediment}/[Th/Ba]_{source\ rock}$ | mass | |
| | | $\alpha_{Rb} = [Th/Rb]_{sediment}/[Th/Rb]_{source\ rock}$ | mass | |
| | | $\alpha^{Al}_E = [Al/E]_{sediment}/[Al/E]_{source\ rock}$, | mass | Garzanti et al., 2013 |
| weathering intensity scale | proportion of trivalent cations | $R^{3+}/(R^{3+}+R^{2+}+M^{+}) = (Fe^{3+}+Al^{3+})/[(Fe^{2+}+Mg^{2+}+Mn^{2+})+(Na^{+}+K^{+}+2\times Ca^{2+})]$ | molar | Meunier et al., 2013 |
| | Si-accumulation index | $4Si=Si/4$; $4Si\%=[Si/4]/([Si/4]+M^{+}+R^{2+})$; $\Delta 4Si\% = [(4Si\%_{weathered\ materials}-4Si\%_{source\ rock})\times 100]/(100-4Si\%_{source\ rock})$ | molar | |
| mafic index of alternation for oxidative condition | | $MIA\text{-}O = 100\times(Al_2O_3+Fe_2O_{3T})/(Al_2O_3+Fe_2O_{3T}+MgO+CaO^*+Na_2O+K_2O)$ | molar | Babechuk et al., 2014 |
| loss chemical weathering proxy | | $LCWP = (CaO^*+Na_2O+MgO)/TiO_2$ | mass | Yang et al., 2006 |
| chemical weathering depletion | | $CDF = 1-Zr_{soil}/Zr_{protolith}$ | mass | Riebe et al., 2004 |
| | | $\tau_{Na} = (Na/Zr)_{soil}/(Na/Zr)_{protolith}-1$ | | Rasmussen et al., 2011 |

*Except $\alpha_E$, $\alpha^{Al}_E$, LCWP and IOL calculated using mass-contents of oxides, all other weathering indices are calculated based on molecular proportion.

CaO* denotes the corrected CaO in silicate minerals following the method of McLennan (1993).

Table 2

Table 2 Statistical results for the correlations of CIA with other weathering indices

| WI | WIP | CIW | PIA | CIX | CPA | LCWP | $\tau_{Na}$ | CDF | MIA-O |
|---|---|---|---|---|---|---|---|---|---|
| $r^2$ | 0.92 | 0.97 | 0.98 | 0.99 | 0.95 | 0.94 | 0.85 | 0.30 | 0.97 |
| P | <0.0001 | <0.0001 | <0.0001 | <0.0001 | <0.0001 | <0.0001 | <0.0001 | <0.0001 | <0.0001 |
| F* | P | P | P | P | P | P | P | P | L |
| C* | Nv | Pv | Pv | Pv | Pv | Nv | Nv | Pv | Pv |
| WI | △4Si% | $R^{3+}/(R^{3+}+R^{2+}+M^{+})$ | | $\alpha_{Ca}$ | $\alpha^{Al}_{Ca}$ | $\alpha_{Na}$ | $\alpha^{Al}_{Na}$ | $\alpha_{K}$ | $\alpha^{Al}_{K}$ |
| $r^2$ | 0.86 | 0.99 | | 0.40 | 0.46 | 0.03 | 0.90 | 0.88 | 0.93 |
| P | <0.0001 | <0.0001 | | <0.0001 | <0.0001 | <0.0000 | <0.0001 | <0.0001 | <0.0001 |
| F* | P | L | | E | E | E | E | E | E |
| C* | Pv | Pv | | Pv | Pv | No* | Pv | Pv | Pv |
| WI | $\alpha_{Sr}$ | $\alpha^{Al}_{Sr}$ | $\alpha_{Mg}$ | $\alpha_{Ba}$ | $\alpha^{Al}_{Ba}$ | $\alpha_{Rb}$ | $\alpha^{Al}_{Rb}$ | F*: regressions are P-polynomial, | |
| $r^2$ | 0.05 | 0.28 | 0.77 | 0.52 | 0.77 | 0.89 | 0.93 | L-linear, E-exponential and | |
| P | <0.0001 | <0.0001 | <0.0001 | <0.0001 | <0.0001 | <0.0001 | <0.0001 | S-single peak; | |
| F* | S | E | E | E | E | E | E | C*: correlations are Pv-positive | |
| C* | Pv | Pv | Pv | Pv | Pv | Pv | Pv | and Nv-negative. | |

*There is no correlation between $\alpha_{Na}$ and CIA.